UV scattering by pores in avian eggshells

Ladouce, M.; Barakat, T.; Su, B. L.; Deparis, O.; Mouchet, S. R.

Published in:
Light in Nature VIII

DOI:
10.1117/12.2567915

Publication date:
2020

Document Version
Publisher's PDF, also known as Version of record

PROCEEDINGS OF SPIE

SPIEDigitalLibrary.org/conference-proceedings-of-spie

UV scattering by pores in avian eggshells

Ladouce, M., Barakat, T., Su, B.-L., Deparis, O., Mouchet, S.

M. Ladouce, T. Barakat, B.-L. Su, O. Deparis, S. R. Mouchet, "UV scattering by pores in avian eggshells," Proc. SPIE 11481, Light in Nature VIII, 114810G (21 August 2020); doi: 10.1117/12.2567915

SPIE.

Event: SPIE Optical Engineering + Applications, 2020, Online Only

UV scattering by pores in avian eggshells

M. Ladouce[a], T. Barakat[b], B.-L. Su[b,c,d], O. Deparis[a] and S. R. Mouchet[a,e]

[a]Department of Physics and Namur Institute of Structured Matter (NISM), University of Namur, Rue de Bruxelles 61, 5000 Namur, Belgium
[b]Laboratory of Inorganic Materials Chemistry (CMI) and Namur Institute of Structured Matter (NISM), University of Namur, Rue de Bruxelles 61, 5000 Namur, Belgium
[c]State Key Laboratory of Advanced Technology for Materials Synthesis and Processing, Wuhan University of Technology, 122 Luoshi Road, Wuhan, Hubei 430070, China
[d]Department of Chemistry and Clare Hall College, University of Cambridge, Herschel Road, Cambridge CB3 9AL, United Kingdom
[e]School of Physics, University of Exeter, Stocker Road, Exeter EX4 4QL, United Kingdom

ABSTRACT

Eggshell is essential for the reproduction of birds. The optical properties of their shells may have an impact on biological functions such as heat and UV protection, recognition by the parents or camouflage. Whereas ultraviolet reflection by bird eggshells has been superficially described in the scientific literature, the physical origin of this phenomenon remains poorly understood. In this article, reflectance peaks in the near UV range were observed by spectrophotometric measurements of hen eggshells. In addition, electron microscopy imaging revealed the presence of pores within the so-called "calcified shell" part (i.e., between *ca.* 20 µm and *ca.* 240 µm deep from the outer surface). The average radii of these pores range from 120 to 160 nm. Mercury intrusion porosimetry allowed to highlight a distribution of pore radii around 175 nm. Numerical and analytical predictions using scattering theory indicate that these pores are responsible for the optical response observed in the UV range.

Keywords: Eggshell, UV scattering, Ultraviolet radiation, Photonics, Natural photonic structures, Nanostructure, Avian eggshell, Cuticle, Ultraviolet reflectance

1. INTRODUCTION

Many bird species are tetrachromatic[1], possessing Short, Medium and Long Wavelength Sensitive (SWS, MWS, LWS) cones whose spectral sensitivity is similar to human being. In addition, a fourth cone, namely the Very Short Wavelength Sensitive (VSWS) cone extends their color vision to ultraviolet (UV) radiation. Therefore, some birds have evolved intraspecific or interspecific communication functions in the UV range. For example, some feathers[2] or hatching skins[3] are known to reflect strongly UV, which plays a role in mate choice or offspring care.

Avian eggshell is a structured material mainly composed of calcite crystallites[4-9]. The outer protein layer is the cuticle covering the so-called calcified shell, which comprises calcareous columns laying on the mammillary layer. The deepest layer is the outer membrane of the egg. The physical properties of avian eggshells favor the embryonic development by allowing, for example, protection from physical damages, controlled gas transfer, bacterial protection and calcium supply[4,10-12]. Their optical properties are also related to biological functions such as heat protection, brood parasitism, and recognition by the parents[1,13-21]. Previous studies reported the link between visual appearance of eggshells in the UV range, and mimicry and rejection mechanisms in the context of brood parasitism[1,20,21].

In a previous work[22], we observed strong UV reflection from beige domestic hen (*Gallus gallus domesticus*) eggshells (Fig. 1a), which appears to arise from light backscattering by air-filled spherical cavities located in the palisade layer of the calcified shell. The total reflectance spectrum of beige hen eggshell (Fig. 1b) reveals two reflectance peaks at *ca.* 252 nm and 314 nm. Dissolving the cuticle[22-25], which may contain pigments responsible for the coloration of eggshells[9,15,26-28], increases the reflectance peak intensities which reach 97% at *ca.* 252 nm and 85% at *ca.* 314 nm.

Light in Nature VIII, edited by Vasudevan Lakshminarayanan, Katherine Creath, Joseph A. Shaw, Proc. of SPIE Vol. 11481, 114810G · © 2020 SPIE
CCC code: 0277-786X/20/$21 · doi: 10.1117/12.2567915

In this article, we characterized the morphological properties of the porous structure of beige hen eggshells. This structure appears to be responsible for the measured UV scattering. Moreover, based on morphological and spectral observations, we performed preliminary calculations using Mie scattering theory and an effective multiple scattering model in order to predict the optical response observed in the UV range.

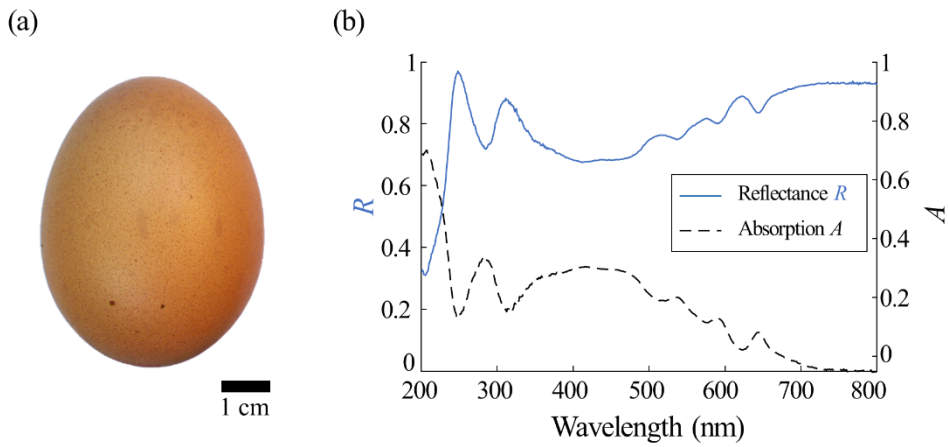

Figure 1. Visual appearance[22] of the beige hen (*G. gallus domesticus*) eggshell (a). The total reflectance and absorption spectra (b) of beige hen eggshell[22] treated with 0.34 M EDTA for 120 min. indicate that the cuticle absorbs incident UV light, whereas the underlying calcified shell scatters UV light so that two reflectance peaks are observed at *ca.* 252 nm and 314 nm.

2. MATERIALS AND METHODS

2.1 Samples

Samples of beige hen eggs ($N = 5$) were bought from retail shops in the UK. Eggshells were separated from their content by piercing small holes at both poles of the shells with a dissection needle. They were dissected and samples were taken from the equatorial areas, allowing the fragments to be as flat as possible. Shell fragments were abundantly rinsed with water.

The cuticle of some eggshell samples was dissolved chemically with 0.34 M (pH between 8.5 and 9) ethylenediaminetetraacetic acid (EDTA) solution[22,23,25]. Samples were laid on the solution surface and were left floating with the cuticle facing the solution. At the end of the treatment, the aqueous residue remaining on the side in contact with EDTA was gently removed with soft paper and the samples were rinsed in distilled water.

2.2 Spectrophotometry

Total transmittance $T(\lambda)$, total reflectance $R(\lambda)$ (Fig. 1b) and absorption $A(\lambda)$ (Fig. 1b) spectra of samples treated with EDTA for 120 min. were measured using a PerkinElmer 750S UV/Vis/NIR spectrophotometer equipped with a 150-mm diameter integrating sphere and a deuterium-tungsten light source. Calibration was performed with a Labsphere SRS-99-020 white reference. The samples approximately measuring 1.5 cm² were placed at the input and output sphere apertures for transmittance and reflectance measurements, respectively, whereas they were suspended at the center of the integrating sphere using an *ad-hoc* sample holder for absorption measurement.

2.3 Electron microscopy

Scanning electron microscopy (SEM) observations of the cross-section of beige hen eggshells were performed with a JEOL 7500F microscope used in secondary electron detection mode. Imaging was performed with a 15 kV acceleration voltage corresponding to a theoretical 1-nm lateral resolution. Eggshell fragments measuring approximately 5 × 5 mm² were positioned vertically on a 90°-angled SEM sample stub using conductive carbon adhesive tape. A thin layer (*ca.* 10 nm) of gold was deposited on the samples to avoid any charging effect.

2.4 Mercury intrusion porosimetry

Porosimetry measurements were performed on eggshells by mercury intrusion using a Micromeritics Autopore IV intrusion porosimeter to assess their pores size distribution. For this purpose, we used sufficiently large (2 × 2 mm²) shell

fragments to fill the sample cup of the penetrometer. The fragments were pre-treated with EDTA for *ca.* 24 h in order to maximize access to the pores by mercury. The outer membrane was removed mechanically.

2.5 Prediction of UV scattering by pores based on Mie scattering theory

Mie scattering theory provides exact expressions of electric and magnetic fields scattered inside and outside of a single homogeneous spherical volume of radius a and refractive index $n_2(\lambda)$ within a surrounding medium of refractive index $n_1(\lambda)$[29]. We could use Mie theory to describe the scattering of UV light by a single air cavity in calcite. However, the porous structure observed in the calcified shell can be modelled as a collection of spherical scatterers randomly distributed in a calcite matrix. An accurate description of light propagation in such a random medium requires to account for each scattering center and interference effects resulting from successive scattering events. As a preliminary approach, we considered a first Born approximation, where scattering events occur independently[30]. In this framework, the scattering mean free path l_t of this effective model of the structure is a function of the wavelength given by

$$l_\mathrm{t}(\lambda;\tilde{a}) = \frac{1}{\rho\sigma_\mathrm{sca}(\lambda;\, a=\tilde{a})} \tag{1}$$

where ρ is the volumetric density of the spheres in the medium and σ_sca is the Mie scattering cross-section of a single sphere of radius $\tilde{a}$.

Total reflectance T_tot of the scattering medium is related, in the first approximation of the multiple scattering theory, to the scattering mean free path l_t as[31]:

$$T_\mathrm{tot}(\lambda) = \frac{l_\mathrm{t}(\lambda)+z_\mathrm{e}(\lambda)}{t+2z_\mathrm{e}(\lambda)} \tag{2}$$

where t is the thickness of the scattering medium and $z_\mathrm{e} = 2l_\mathrm{t}(\lambda)\alpha(\lambda)/3$ is the extrapolation length. The coefficient α is a correction factor accounting for multiple internal reflections. Equations 1 and 2 allow us to compare the scattering mean free path calculated from the effective model theory and the one extracted from the total transmittance measurement, respectively. However, total transmittance measurements are performed on eggshell samples, thickness d (*ca.* 400 µm) of which is greater than the thickness t of the scattering layers (*ca.* 220 µm) located in the palisade layer. In order to use a transmittance spectrum close to the real transmittance of the scattering medium only, we applied a Beer-Lambert correction to T_tot that eliminates absorption in non-scattering layers, based on the assumption that the extinction coefficient κ_ext is constant along the whole eggshell cross-section:

$$T_\mathrm{tot}^\mathrm{corr}(\lambda) = T_\mathrm{tot}(\lambda)\mathrm{e}^{(d-t)\kappa_\mathrm{ext}(\lambda)}. \tag{3}$$

The extinction coefficient κ_ext was derived from absorption measurement according to:

$$\kappa_\mathrm{ext}(\lambda) = \frac{-\ln(10)\log_{10}\left(1-A(\lambda)\right)}{d}. \tag{4}$$

We also calculated the backscattering efficiency Q_b (function of a and λ) of a single sphere, defined as the ratio between the backscattering cross-section σ_b derived from Mie theory[29] and the area of the equatorial section of the sphere.:

$$Q_\mathrm{b}(\lambda, a, n) = \frac{\sigma_\mathrm{b}(\lambda,a,m)}{\pi a^2} \tag{5}$$

with $m = m(\lambda) = n_2/n_1$. In the framework of the selected effective model, we assessed the backscattering efficiency of the whole scattering medium as the average of each single spherical scatterer efficiency weighted by a given radius distribution $\gamma(a)$ of the spheres. This quantity, called *weighted average of backscattering efficiencies*, is a function of the wavelength and is defined as:

$$S_\mathrm{b}(\lambda) = \frac{\int_{a_1}^{a_2} Q_\mathrm{b}(\lambda,a,m)\gamma(a)\,da}{\int_{a_1}^{a_2} \gamma(a)\,da} \tag{6}$$

Similar quantity could be calculated based on the scattering efficiency[22] $Q_\mathrm{Sca} = \sigma_\mathrm{Sca}/\pi a^2$, but we focused here on backscattering only in order to compare and discuss the spectral contributions of $S_\mathrm{b}(\lambda)$ to experimental peaks of the total reflectance spectra in the UV range.

3. RESULTS AND DISCUSSIONS

3.1 Morphological characterization of the porous structure

SEM observations of eggshell cross-sections (Fig. 2a-c) allow to identify pores as circular pits assumed to correspond to spherical void cavities. Pores are only observed in the palisade layer over a thickness of *ca*. 220 µm, from *ca*. 20 µm below the outer surface (Fig. 2a). Software-assisted image analysis using the Analyze Particles subroutine of ImageJ[32] lead to a pore surface density of 1.22 μm^{-2} and an average radius of 145 ± 54 nm.

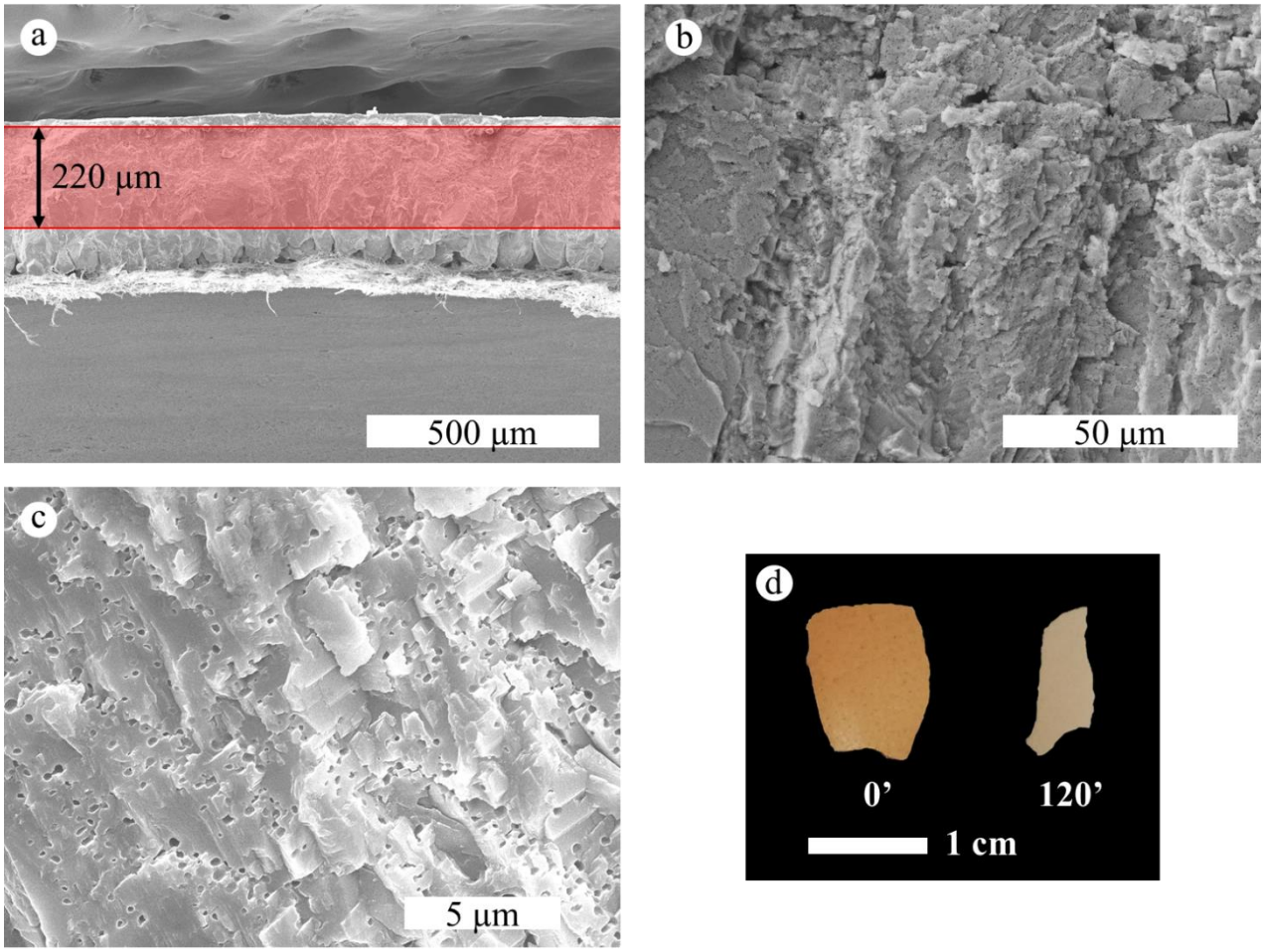

Figure 2. SEM observations (a-c) of the beige hen eggshell cross-section revealing the presence of pores in the calcified shell. Global view of the cross section (a); Magnification on the palisade layer, revealing the pores (darker spots) (b); more detailed overview of the pores (c). The red area (a) approximately indicates the position of the porous region. Comparative picture (d) between beige hen eggshell sample treated for 120 min with 0.34 M EDTA solution (right) and untreated (left). This process slowly thins down the cuticle that is known to contain pigments[15,22,23,25]. One can observe a loss in pigmentation.

Adsorption isotherm of analyzed samples was obtained by mercury intrusion porosimetry. The curve (Fig. 3a) corresponds to a Type IV isotherm, with a central plateau usually associated with porosity[33]. The pore diameter distribution (Fig. 3b) was fitted with a Gaussian function (Fig. 3c) to the peak observed in the pore size range relevant for our analysis. The resulting Gaussian function had an average radius of 204 ± 4 nm. A second peak is observed for larger sizes with a diameter of *ca*. 2 µm. These sizes are likely due to interstices between calcareous columns in the palisade layer or to the sample surface roughness.

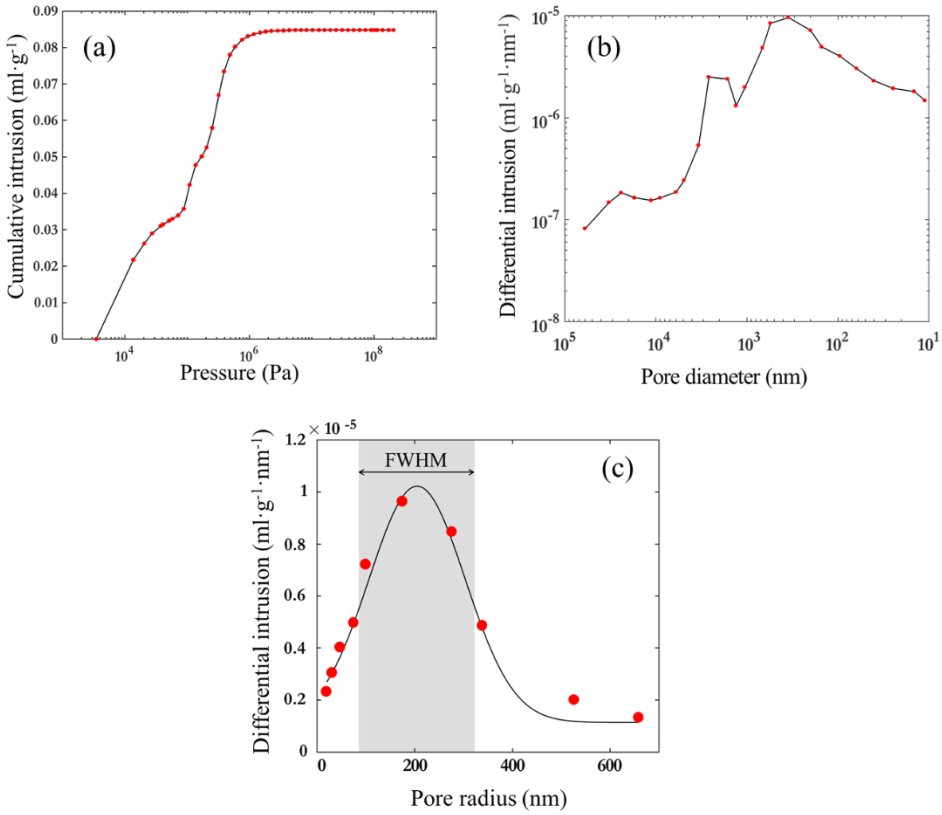

Figure 3. Mercury intrusion as a function of the applied external pressure (a) corresponding to a type IV isotherm in the IUPAC classification[33]. Mercury intrusion porosimetry allows to assess the pore diameter distribution (b) which is fitted by a Gaussian function (c) in the region of interest. The full width at half maximum (FWHM) is 236.6 nm. The standard error of differential intrusion measurements was ± 1%.

3.2 Scattering properties

The scattering mean free path extracted from measurement of the total transmittance (Fig. 4a) and the one calculated from Mie scattering cross-section of a single scatterer (Fig. 4b) exhibit relatively comparable (<1 µm) values in the UV range. This demonstrate the reliability of an effective model in this range.

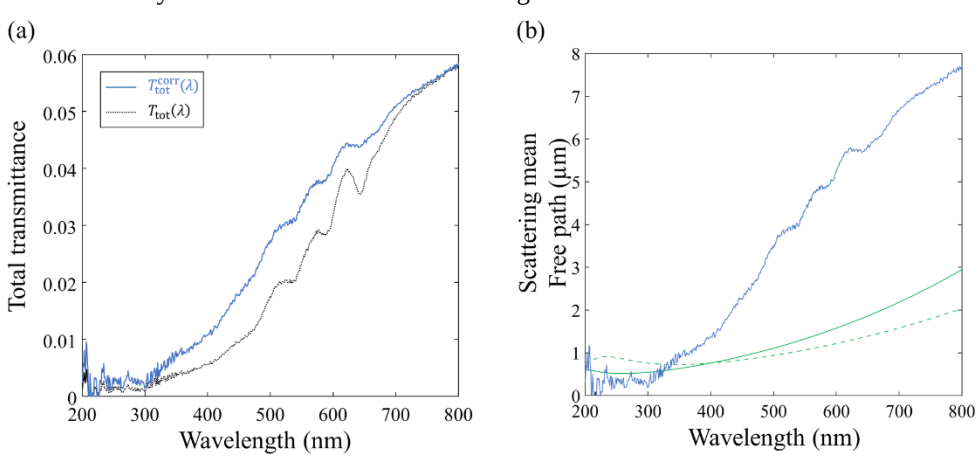

Figure 4. Total transmittance spectra (a) before (black solid line) and after Beer-Lambert absorption correction (blue solid line). Comparison (b) between the scattering mean free path $l_t(\lambda)$ calculated from Mie scattering cross-section of a single scatterer with a = 145 nm (green solid line) and a = 205 nm (green dashed line) and the mean free path calculated from transmittance measurements (blue line).

The backscattering efficiency $Q_{\mathrm{b}}(\lambda, a, m)$ was calculated for two different refractive indices n_1, the first corresponding to the average between the ordinary and extraordinary indices of crystalline calcite[34] $n_1(\lambda) = \bar{n}_{\mathrm{calcite}}(\lambda) \stackrel{\mathrm{def}}{=} [n^{\mathrm{o}}_{\mathrm{calcite}}(\lambda) + n^{\mathrm{e}}_{\mathrm{calcite}}(\lambda)]/2$ and the second being chosen constant $n_1(\lambda) = 1.63$. Since spheres are composed of air, the refractive index of the pores was $n_2(\lambda) = 1$. The calculated backscattering efficiency displays multiple resonance modes (Fig. 5a,b) whose wavelength and radius dependence appears at first glance as barely affected by the refractive index. The resulting weighted averages of backscattering efficiencies exhibit local maxima close to the total reflectance peak wavelengths (Fig. 5c,d). Since the dispersion relations of calcite tends to decrease the refractive indices with the wavelength following a monotonic function, the first local maximum of S_{b} calculated with $\bar{n}_{\mathrm{calcite}}(\lambda)$ (Fig. 5c) has a higher intensity than the one with the constant refractive index (Fig. 5d) but does not stand out as much from the spectrum. Although the reflectance R and S_{b} cannot be directly compared, we can compare the ratio between the peak intensities (at λ_{P1}= 248 nm and λ_{P2}=311 nm) for both curves, assuming a linear scaling between both quantities: $r_R = R(\lambda_{P1})/R(\lambda_{P2}) = 1.10$; $r_{S1} = S_{\mathrm{b}}(\lambda_{\mathrm{P1}}, \bar{n}_{\mathrm{calcite}})/S_{\mathrm{b}}(\lambda_{\mathrm{P2}}, \bar{n}_{\mathrm{calcite}}) = 1.10$ and $r_{S2} = S_{\mathrm{b}}(\lambda_{\mathrm{P1}}, n_1 = 1.63)/S_{\mathrm{b}}(\lambda_{\mathrm{P2}}, n_1 = 1.63) = 1.03$. All three ratios are close but r_{S1} perfectly matches r_R, which is expected since the averaged refracting index is much more realistic than the constant one. This result shows that the refractive index of the surrounding media (namely, calcite) is a sensitive parameter. The agreement between r_R and r_{S1}indicates that the observed response in the UV range is due to multiple backscattering.

Furthermore, we calculated the spatial distribution of electric field intensity around a sphere (a = 205 nm) based on Mie theory for λ = 206 nm (i.e., around a backscattering resonance mode, Fig. 6a) and 345 nm (namely, outside any backscattering resonance mode, Fig. 6b) using the dispersive refractive index $\bar{n}_{\mathrm{calcite}}(\lambda)$. The field intensity corresponding to a wavelength around resonance (Fig. 6a) shows a pattern mainly concentrated in the incident direction, i.e. typical of backscattering, whereas it is much more scattered around the sphere for a wavelength outside any resonance mode. The field intensity is overall lower in the shadow of the sphere in the case λ = 206 nm.

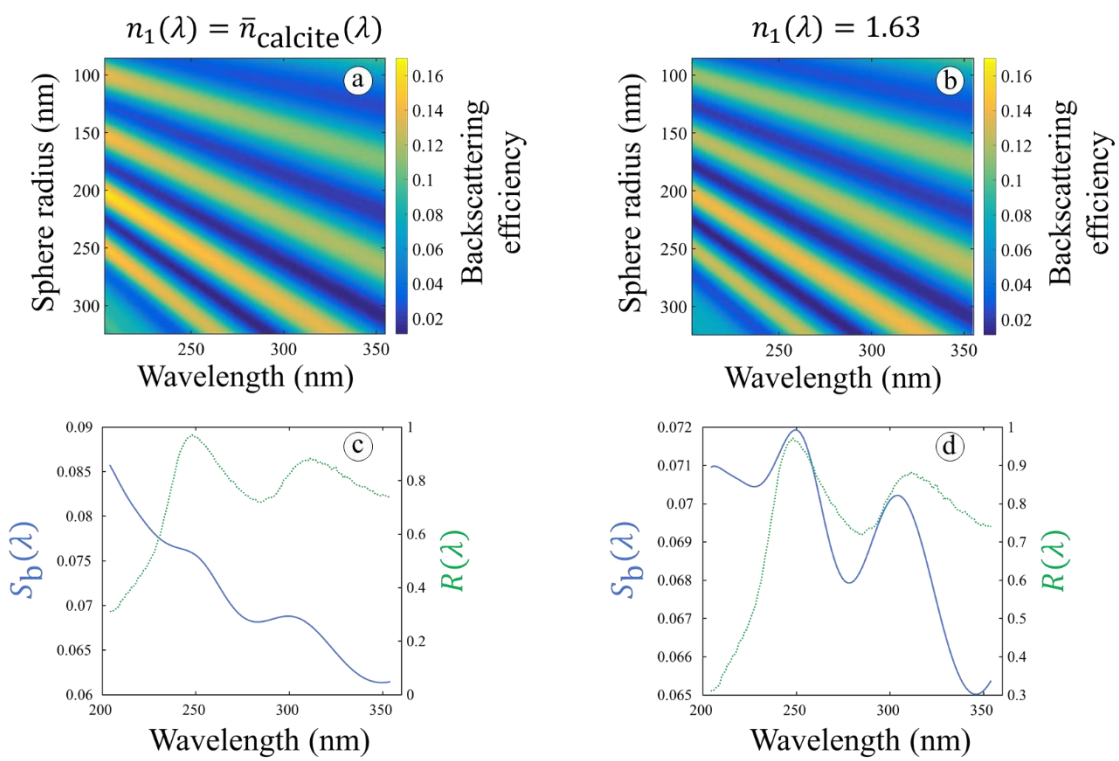

Figure 5. The Mie backscattering efficiency maps (a,b) exhibit several resonance modes depending on the wavelength and the sphere radius . The efficiency is globally slightly weaker for the constant refractive index case (b). The weighted average of backscattering efficiencies (c,d blue solid lines) and measured reflectance spectrum (c,d green dashed lines) show similar wavelength dependencies which are less marked in the dispersive refractive index case (c).

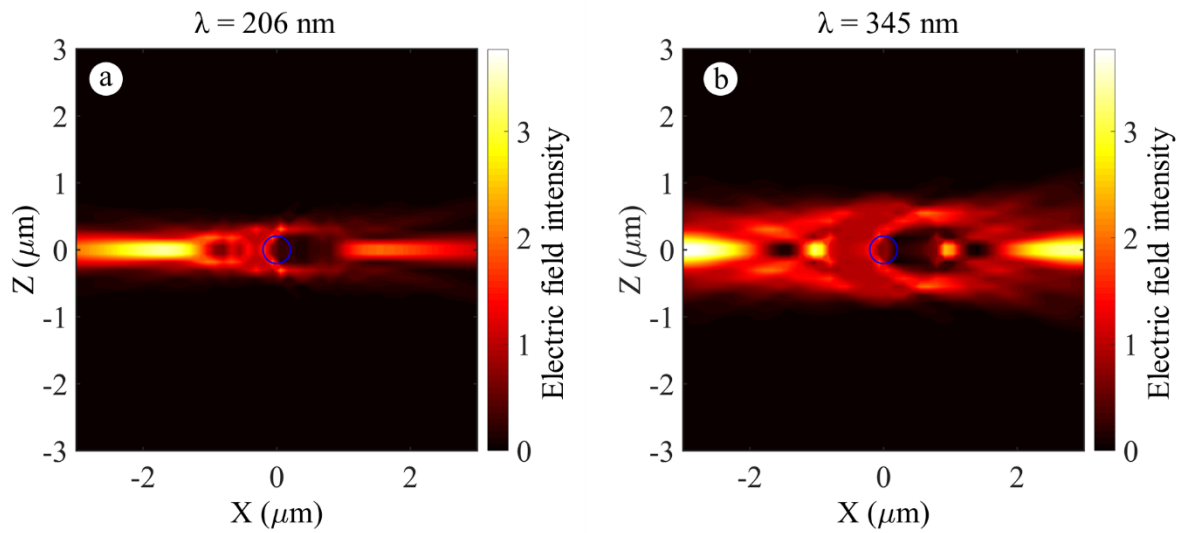

Figure 6. Spatial distribution of scattered electric field intensity inside and outside the sphere (a = 205 nm) for λ = 206 nm (a) and 345 nm (b). Calculations were performed using 22 harmonic terms. Incident light comes from the left. The blue circle corresponds to the equatorial section of the sphere.

4. CONCLUSIONS

The strong UV reflection observed in beige hen (*G. gallus domesticus*) eggshells treated with EDTA solutions originates from the scattering porous structure embedded within the calcified shell. In addition, the eggshell cuticle partly absorbs UV radiation. Such optical properties may have an impact on biological functions related to UV signaling and perception in this wavelength range. SEM observations of the cross-section of the shell revealed spherical cavities in the calcified shell. Their size distribution was quantified by mercury intrusion porosimetry. Predictions of the optical properties of this porous structure in hen eggshells were performed by considering an effective model where multiple scattering events by each spherical cavity are assumed independent. The comparison between the measured total reflectance of the eggshell and predictions of the Mie backscattering efficiency weighted by a Gaussian function accounting for the size distribution measured by mercury intrusion porosimetry indicates that the pores observed in the palisade layer of the calcified shell are produce multiple Mie scattering events.

ACKNOWLEDGEMENTS

The authors thank C. Charlier (Electron Microscopy Service, UNamur) for technical support during electron microscopy observations, respectively. S.R.M. was supported by the Belgian National Fund for Scientific Research (FRS-FNRS) as a Postdoctoral Researcher (91400/1.B.309.18F). This research was also supported by FRS-FNRS through the Researchers' Credit CC 1.5075.11F. This research used resources of the Technological Platform High Performance Computing (PTCI) (http://www.ptci.unamur.be) located at UNamur and the resources of the Electron Microscopy Service (SME) of UNamur (http://www.unamur.be/en/sevmel). PTCI is supported by FNRS-FRFC, the Walloon Region and UNamur (Conventions No. 2.5020.11, GEQ U.G006.15, 1610468 and RW/GEQ2016). PTCI and SME are members of the "Consortium des Équipements de Calcul Intensif (CÉCI)" (http://www.ceci-hpc.be) and the Technological Platform Morphology - Imaging (MORPH-IM) of UNamur, respectively.

REFERENCES

[1] Stoddard, M. C. and Stevens, M., "Avian vision and the evolution of egg color mimicry in the common cuckoo," Evolution (N. Y). **65**(7), 2004–2013 (2011).

[2] Siitari, H. and Huhta, E., "Individual color variation and male quality in pied flycatchers (Ficedula hypoleuca): A role of ultraviolet reflectance," Behav. Ecol. **13**(6), 2002.
[3] Jourdie, V., Moureau, B., Bennett, A. T. D. and Heeb, P., "Ultraviolet reflectance by the skin of nestlings," Nature **431**(7006), 262 (2004).
[4] Tyler, C., "Avian Egg Shells: Their Structure and Characteristics," [International Review of General and Experimental Zoology], W. J. L. Felts and R. J. Harrison, Eds., Academic Press, 81–130 (1969)
[5] Tullett, S. G., "The porosity of avian eggshells," Comp. Biochem. Physiol. -- Part A Physiol. **78**(1), 5–13 (1984).
[6] Panheleux, M., Bain, M., Fernandez, M. S., Morales, I., Gautron, J., Arias, J. L., Solomon, S. E., Hincke, M. and Nys, Y., "Organic matrix composition and ultrastructure of eggshell: A comparative study," Br. Poult. Sci. **40**(2), 240–252 (1999).
[7] Richards, P. D. G. and Deeming, D. C., "Correlation between shell colour and ultrastructure in pheasant eggs," Br. Poult. Sci. **42**(3), 338–343 (2001).
[8] Mikhailov, K. E., [Avian eggshells: an atlas of scanning electron micrographs] (1997).
[9] Ostertag, E., Scholz, M., Klein, J., Rebner, K. and Oelkrug, D., "Pigmentation of White, Brown, and Green Chicken Eggshells Analyzed by Reflectance, Transmittance, and Fluorescence Spectroscopy," ChemistryOpen **8**(8), 1084–1093 (2019).
[10] Ketta, M. and Tůmová, E., "Eggshell structure, measurements, and quality-affecting factors in laying hens: a review," Czech J. Anim. Sci **61**(7), 299–309 (2016).
[11] Stoddard, M. C., Yong, E. H., Akkaynak, D., Sheard, C., Tobias, J. A. and Mahadevan, L., "Avian egg shape: Form, function, and evolution," Science (80-.). **356**(6344), 1249–1254 (2017).
[12] D'Alba, L., Jones, D. N., Badawy, H. T., Eliason, C. M. and Shawkey, M. D., "Antimicrobial properties of a nanostructured eggshell from a compost-nesting bird," J. Exp. Biol. **217**(7), 1116–1121 (2014).
[13] Avilés, J. M., Soler, J. J. and Pérez-Contreras, T., "Dark nests and egg colour in birds: a possible functional role of ultraviolet reflectance in egg detectability," Proc. R. Soc. B Biol. Sci. **273**(1603), 2821–2829 (2006).
[14] Cherry, M. I. and Bennett, T. D., "Egg colour matching in an African cuckoo, as revealed by ultraviolet-visible reflectance spectrophotometry," Proc. R. Soc. London. Ser. B Biol. Sci. **268**(1467), 565–571 (2001).
[15] Hauber, M. E., Bond, A. L., Kouwenberg, A.-L., Robertson, G. J., Hansen, E. S., Holford, M., Dainson, M., Luro, A. and Dale, J., "The chemical basis of a signal of individual identity: shell pigment concentrations track the unique appearance of Common Murre eggs," J. R. Soc. Interface **16**(153), 20190115 (2019).
[16] Moreno, J. and Osorno, J. L., "Avian egg colour and sexual selection: Does eggshell pigmentation reflect female condition and genetic quality?," Ecol. Lett. **6**(9), 803–806 (2003).
[17] Kilner, R. M., "The evolution of egg colour and patterning in birds," Biol. Rev. Camb. Philos. Soc. **81**(3), 383–406 (2006).
[18] Cassey, P., Thomas, G. H., Portugal, S. J., Maurer, G., Hauber, M. E., Grim, T., Lovell, P. G. and Mikšík, I., "Why are birds' eggs colourful? Eggshell pigments co-vary with life-history and nesting ecology among British breeding non-passerine birds," Biol. J. Linn. Soc. **106**(3), 657–672 (2012).
[19] Maurer, G., Portugal, S. J., Hauber, M. E., Mikšík, I., Russell, D. G. D. and Cassey, P., "First light for avian embryos: eggshell thickness and pigmentation mediate variation in development and UV exposure in wild bird eggs," Funct. Ecol. **29**(2), B. Tschirren, Ed., 209–218 (2015).
[20] Cassey, P., Honza, M., Grim, T. and Hauber, M. E., "The modelling of avian visual perception predicts behavioural rejection responses to foreign egg colours," Biol. Lett. **4**(5), 515–517 (2008).
[21] Stoddard, M. C. and Stevens, M., "Pattern mimicry of host eggs by the common cuckoo, as seen through a bird's eye," Proc. R. Soc. B Biol. Sci. **277**(1686), 1387–1393 (2010).
[22] Ladouce, M., Barakat, T., Su, B.-L., Deparis, O. and Mouchet, S. R., "Scattering of ultraviolet light by avian eggshells," Faraday Discuss. (2020), doi: 10.1039/D0FD00034E.
[23] Fecheyr-Lippens, D. C., Igic, B., D'Alba, L., Hanley, D., Verdes, A., Holford, M., Waterhouse, G. I. N., Grim, T., Hauber, M. E. and Shawkey, M. D., "The cuticle modulates ultraviolet reflectance of avian eggshells," Biol. Open **4**(7), 753–759 (2015).
[24] Igic, B., Fecheyr-Lippens, D., Xiao, M., Chan, A., Hanley, D., Brennan, P. R. L., Grim, T., Waterhouse, G. I. N., Hauber, M. E. and Shawkey, M. D., "A nanostructural basis for gloss of avian eggshells," J. R. Soc. Interface **12**(103), 20141210 (2015).
[25] D'Alba, L., Torres, R., Waterhouse, G. I. N., Eliason, C., Hauber, M. E. and Shawkey, M. D., "What does the eggshell cuticle do? A functional comparison of avian eggshell cuticles," Physiol. Biochem. Zool. **90**(5), 588–

599 (2017).
[26] Keneddy, G. Y. and Vevers, H. G., "Eggshell pigments of the araucano fowl," Comp. Biochem. Physiol. -- Part B Biochem. **44**(1), 11–25 (1973).
[27] Kennedy, G. Y. and Vevers, H. G., "A survey of avian eggshell pigments," Comp. Biochem. Physiol. -- Part B Biochem. **55**(1), 117–123 (1976).
[28] Sparks, N. H. C., "Eggshell Pigments–from Formation to Deposition," Avian Biol. Res. **4**(4), 162–167 (2011).
[29] Bohren, C. F. and Huffman, D. R., "Absorption and Scattering by a Sphere," [Absorption and Scattering of Light by Small Particles], Wiley-VCH Verlag GmbH, Weinheim, Germany, 82–129 (2007).
[30] Akkermans, E. and Montambaux, G., [Mesoscopic physics of electrons and photons], Cambridge University Press (2007).
[31] Burresi, M., Cortese, L., Pattelli, L., Kolle, M., Vukusic, P., Wiersma, D. S., Steiner, U. and Vignolini, S., "Bright-white beetle scales optimise multiple scattering of light," Sci. Rep. **4**(1), 1–8 (2014).
[32] Schneider, C. A., Rasband, W. S. and Eliceiri, K. W., "NIH Image to ImageJ: 25 years of image analysis," Nat. Methods **9**(7), 671–675 (2012).
[33] Thommes, M., Kaneko, K., Neimark, A. V., Olivier, J. P., Rodriguez-Reinoso, F., Rouquerol, J. and Sing, K. S. W., "Physisorption of gases, with special reference to the evaluation of surface area and pore size distribution (IUPAC Technical Report)," Pure Appl. Chem. **87**(9–10), 1051–1069 (2015).
[34] Ghosh, G., "Dispersion-equation coefficients for the refractive index and birefringence of calcite and quartz crystals," Opt. Commun. **163**(1), 95–102 (1999).